Thermal conductivity and accommodation coefficient of spin-polarized atomic-hydrogen gas

M. J. Yoo* and T. J. Greytak
Department of Physics and Center for Materials Science and Engineering, Massachusetts Institute of Technology, Cambridge, Massachusetts 02139
(Received 27 January 1995)

The thermal conductivity of a spin-polarized atomic-hydrogen gas and its accommodation coefficient on saturated superfluid ^{4}He films have been determined experimentally using a cell comprised of coaxial cylinders. The thermal conductivity was measured for temperatures $0.3 < T < 0.4$ K and for magnetic fields $4.00 < H < 7.00$ T. The value of the thermal conductivity for spin-polarized hydrogen is 3×10^{-3} W/K m for $T = 0.3$ K and $H = 7.00$ T. The measured thermal conductivity is independent of the applied magnetic field, and its magnitude and temperature dependence are in agreement with *ab initio* calculations for a paramagnetic Bose gas model. No evidence for anomalous transport due to thermal fluctuations in the gas magnetization has been observed. The accommodation coefficient for spin-polarized hydrogen upon saturated superfluid ^{4}He films for $0.2 < T < 0.4$ K and $3.00 < H < 7.00$ T was found to be independent of the applied magnetic field and to be given by the expression $a_c = (0.56 \pm 0.06)T$. This value is in agreement with previous measurements of the accommodation and sticking coefficients.

I. INTRODUCTION

The thermal transport phenomena in spin-polarized atomic-hydrogen gas (denoted H↓) allow one to investigate the interactions between atoms in the gas. The thermal conductivity of spin-polarized hydrogen is a sensitive probe of the cross section for elastic collisions between hydrogen atoms. These elastic collision cross sections are determined by the H-H interatomic potential and the quantum statistics of the colliding atoms. At the same time, the thermal accommodation of H↓ on saturated superfluid ^{4}He films allows one to investigate the quantum-mechanical interaction between an atom and a surface. Both these phenomena are of growing interest as further progress is made towards the degenerate regime (Bose-Einstein condensation) in spin-polarized hydrogen.

Over the past two decades increasingly more sophisticated models for the thermal conductivity of spin-polarized hydrogen have been developed. Early thermodynamic investigations[1,2] suggested that the hard-sphere Bose gas model provided an approximate description of the kinetic phenomena in H↓. Lhuillier and Laloë[3] then reported *ab initio* calculations for the thermal conductivity and viscosity of spin-polarized hydrogen which accounted for the precise H-H interatomic interaction potential and the nuclear spin statistics of the atoms. Recently, Bashkin[4] suggested that the interaction of a hydrogen atom's nuclear spin with thermal fluctuations of the total nuclear magnetization produces anomalously low values of the thermal conductivity and viscosity in H↓. We shall review these theoretical models in greater detail in Sec. II.

Surprisingly, elastic collision processes in H↓ have never been quantitatively investigated in the laboratory. Approximate values of the thermal conductivity for spin-polarized hydrogen have been observed by several groups, usually as a byproduct of the measurements of other physical quantities. Such values were in order-of-magnitude agreement with hard-sphere Bose gas models. However, since these measurements were performed in poorly defined geometries and for imperfectly understood densities and nuclear polarizations, they afford only qualitative comparison with theoretical predictions.

We report in this paper a measurement of the thermal conductivity of spin-polarized hydrogen performed in a dedicated experimental cell with coaxial cylinder geometry. Our measurements investigate the thermal transport of H↓ for a wide range of temperatures, magnetic fields, densities, and nuclear polarizations. We find values of the thermal conductivity in direct agreement with the paramagnetic Bose gas calculations of Lhuillier and Laloë.[3] Furthermore, we find no evidence for magnetic anomalies in the thermal conductivity. A brief review of the theoretical predictions for transport in H↓ is given in Sec. II, our experimental apparatus and procedure are described in Secs. III and IV, and a detailed discussion of our results is presented in Sec. V.

As a natural consequence of our measurement procedure, we were also able to measure the thermal accommodation coefficient of spin-polarized hydrogen upon a saturated superfluid helium film. Recently, a great deal of theoretical work has focused upon the interaction between hydrogen atoms and liquid-helium surfaces. Much of this work has been motivated by the unusual behavior predicted for a hydrogen atom incident upon superfluid helium surfaces. The sticking probability, defined as the probability that an incident atom makes a transition to a bound surface state, is expected to vanish in the limit of zero incident energy. This counterintuitive result, known as quantum reflection, is attributed to a mismatch between the incident atom and bound-state wave functions and is believed to be a universal phenomenon in low-energy gas-surface interactions.

The accommodation coefficient measures the incomplete equilibration between a gas and a surface; it should also exhibit unusual low-energy behavior. If one assumes

0163-1829/95/52(10)/7215(15)/$06.00 ©1995 The American Physical Society

that energy is transferred between a gas atom and the surface only by sticking events, the accommodation coefficient as a function either of gas temperature or incident atom energy can be directly computed from the sticking probability. Our measurements of the accommodation coefficient are in excellent agreement with previous measurements of the accommodation coefficient[5] as well as previous measurements of the sticking probability[6] for the H↓-superfluid ^{4}He system. These results are discussed further in Sec. V.

II. THEORETICAL PREDICTIONS

A. Background

A gas of hydrogen atoms may be stabilized against the recombination reaction

$$H+H\rightarrow H_2+4.8\ \text{eV} \tag{1}$$

by parallel alignment of their electron spins, for example in an external magnetic field. This system is known as spin-polarized atomic hydrogen (denoted H↓ or H↑) and was first created in the laboratory[7] in a superfluid helium-lined cell within a region of high static magnetic field. H↓ is a weakly interacting Bose gas and is believed to remain gaseous down to $T=0$ K. Furthermore, for sufficiently high densities and low temperatures spin-polarized hydrogen is expected to undergo a transition to the degenerate regime (Bose Einstein condensation or BEC). The transition temperature for BEC in weakly interaction Bose gases is nearly identical to the result for the ideal Bose gas, which is given by the relation

$$T_c=\frac{h^2}{2\pi mk}\left[\frac{n}{2.612}\right]^{2/3} . \tag{2}$$

Here n is the number density of the gas. We refer the reader to the review articles by Greytak and Kleppner[8] and Silvera and Walraven[9] for a comprehensive survey of research on spin-polarized hydrogen.

B. Hyperfine states of hydrogen

Consider a ground-state hydrogen atom in the presence of a static, uniform magnetic field. When we consider the Zeeman energies of the electron and proton spins as well as the hyperfine interaction between these two spins, we find that the 1s ground state splits into four hyperfine states, conventionally labeled a through d in order of increasing energy. The spin wave functions of the hyperfine states are written in the $|m_s m_i\rangle$ representation as

$$\begin{aligned}
|a\rangle &= \cos\theta_m|\downarrow\uparrow\rangle-\sin\theta_m|\uparrow\downarrow\rangle ,\\
|b\rangle &= |\downarrow\downarrow\rangle ,\\
|c\rangle &= \cos\theta_m|\uparrow\downarrow\rangle+\sin\theta_m|\downarrow\uparrow\rangle ,\\
|d\rangle &= |\uparrow\uparrow\rangle .
\end{aligned} \tag{3}$$

The mixing angle θ_m is given by the relation

$$\tan 2\theta_m=\frac{E_{\text{hyp}}}{(\gamma_e+\gamma_p)H}=\frac{0.0506\ \text{T}}{H} , \tag{4}$$

where $E_{\text{hyp}}=h\times 1.402$ GHz is the zero field hyperfine energy and γ_e and γ_p are the electron and proton gyromagnetic ratios for hydrogen.

In the high field limit, the mixing angle θ_m is small and the hyperfine states may be written in approximate form as

$$\begin{aligned}
|a\rangle &= |\downarrow\uparrow\rangle-\theta_m|\uparrow\downarrow\rangle ,\\
|b\rangle &= |\downarrow\downarrow\rangle ,\\
|c\rangle &= |\uparrow\downarrow\rangle+\theta_m|\downarrow\uparrow\rangle ,\\
|d\rangle &= |\uparrow\uparrow\rangle .
\end{aligned} \tag{5}$$

In this limit, the electron and proton spins are nearly decoupled. The electron spins of the a and b states are almost completely aligned antiparallel to the magnetic field. When placed in a magnetic field gradient, a and b atoms feel a force accelerating them towards regions of strong magnetic field. Conversely the c and d atoms are nearly aligned parallel to the magnetic field and are attracted to regions of weak magnetic field. Spin-polarized atomic hydrogen composed of a and b atoms is denoted H↓, while H↑ is used to represent a collection of c and d atoms. As the work in this paper involves H↓, we will restrict our discussion of spin-polarized hydrogen to gases of a and b atoms unless otherwise noted.

C. Interatomic potential

The interaction potential for a pair of ground-state hydrogen atoms in a spatially uniform magnetic field may be written as a sum of several terms:

$$V(r)=V_{\text{Coulomb}}+V_{\text{Zeeman}}+V_{\text{hyperfine}}+V_{\text{dipole}} . \tag{6}$$

The V_{Coulomb} term represents the interaction of the electron and proton charges of both atoms, and it is the dominant contribution to the pair potential. Using a variational approach, Kolos and Wolniewicz performed *ab initio* calculations of V_{Coulomb} for two ground-state hydrogen atoms.[10–13] Their results for the total electron spin singlet ($S=0$) and triplet ($S=1$) interactions are the most accurate calculations of any known interatomic potential (see Fig. 1). The singlet potential $^1\Sigma_g^+$ is strongly attractive, with a well depth of approximately 55 000 K. It supports the bound states of the H_2 molecule. On the other hand, the triplet potential $^3\Sigma_u^+$ is weakly repulsive and permits the stabilization of H↓ against direct molecular recombination. It possesses a shallow 6.5-K-deep well discernible in the expanded view in Fig. 1. Although it supports no bound molecular states, this faintly attractive well strongly influences the low-energy scattering of a pair of hydrogen atoms.

The electron spins influence the Coulomb energy only by determining the symmetry of the spatial wave function, while the nuclear spins play no role whatsoever in V_{Coulomb}. Kolos and Wolniewicz have also disregarded the motion of the nuclei (Born-Oppenheimer approximation) in their calculations of $^1\Sigma_g^+$ and $^3\Sigma_u^+$.

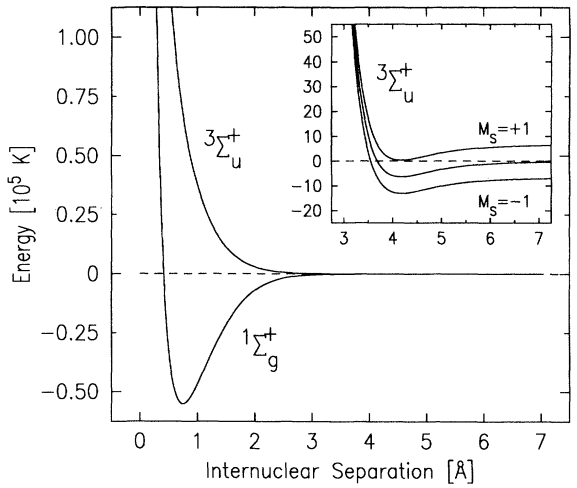

FIG. 1. H-H singlet and triplet interaction potentials in zero magnetic field. Inset: expanded view of the triplet attractive well illustrating the Zeeman effect for $H = 10$ T.

The V_{Zeeman} term represents the interaction between the proton and electron magnetic moments and an external magnetic field. For a magnetic field of 10 T, the electronic Zeeman energy introduces an energy shift of approximately 6.7 K to the triplet potential curves (see Fig. 1). The singlet potential is unaffected if we ignore the nuclear spin. Due to the difference in mass, the Zeeman effect is nearly 3 orders of magnitude smaller for the protons than the electrons. Both the electron and proton Zeeman shifts are independent of the internuclear distance r.

The electron and proton spins also contribute to the interaction potential through the hyperfine energy. This interaction is rather weak, as the hyperfine energy E_{hyp} corresponds to a temperature of approximately 70 mK. If we neglect the weak hyperfine interaction of proton and electron spins on different atoms, then $V_{\text{hyperfine}}$ is independent of the internuclear separation.

The V_{dipole} term includes the magnetic dipole-dipole interactions of the electron and proton spins. The electron-electron dipole energy is the strongest contribution to V_{dipole} and is roughly 20 mK in the vicinity of the shallow attractive well of the triplet Coulomb potential. V_{dipole} is therefore also a weak perturbation of the dominant Coulomb energy.

This description of the interatomic potential applies quite generally to a gas of ground-state hydrogen atoms in a uniform magnetic field. Let us now confine our discussion to H↓, an atomic hydrogen gas composed of the high field seeking hyperfine states a and b. The b atoms are in a pure electron and proton spin state ($|\downarrow\downarrow\rangle$), while the a atoms have a small admixture of the opposite electron spin component ($|\downarrow\downarrow\rangle - \theta_m|\uparrow\downarrow\rangle$).

In the high field limit, the a-a, a-b, and b-b Coulomb energies are given by the triplet potential $^3\Sigma_u^+$ and are all perturbed by the $M_s = -1$ Zeeman shift as well as the hyperfine energies of the individual atoms. Since these contributions are independent of the internuclear separation r, they are equivalent to a redefinition of the energy zero and may be safely ignored in collisional processes. We disregard the dipole-dipole interactions because they are at least 2 orders of magnitude smaller than the Coulomb interaction.

We shall make the approximation in the high-field limit that the a-a, a-b, and b-b interaction potentials are entirely Coulombic in nature and are all given by the triplet $^3\Sigma_u^+$ interaction calculated by Kolos and Wolniewicz for zero magnetic field. Note that this assumption implies the pair interaction potentials in H↓ are independent of the electron and proton spin states of the atoms.

This grossly simplified picture of the interaction energies in H↓ is suitable for transport calculations, since the Coulomb interaction is the dominant source of elastic collisions in the gas. However for description of phenomena in H↓ involving inelastic collisions, one generally includes the spin-dependent interactions we have neglected.

D. Collision cross sections

Since the interaction potential $V(r)$ is spherically symmetric, the orbital angular momentum l is a good quantum number during collisions. We consider scattering via different angular-momentum channels separately and investigate binary collisions in the gas using the method of partial waves.

The phase shift $\delta_l(k)$ associated with the partial wave of angular momentum l is a function of the relative incident wave vector of the collision. Lhuillier[3] has calculated the phase shifts for the $^3\Sigma_u^+$ potential of Kolos and Wolniewicz numerically. The high-energy behavior of δ_l is primarily determined by the repulsive core of the $^3\Sigma_u^+$ potential. For energies small compared to the well depth ($k \ll 0.35$ Å^{-1}) the attractive well moderates the repulsive effects of the hard core.

Friend and Etters[14] and Lantto and Nieminen[15] have determined the s-wave scattering length a in spin-polarized hydrogen to be

$$a = -\lim_{k\to 0}\frac{\delta_0(k)}{k} = 0.72 \text{ Å} . \tag{7}$$

Since a is positive and small, the interaction between hydrogen atoms in H↓ is weakly repulsive.

The cross section for binary elastic collisions in spin-polarized hydrogen are then easily computed from the phase shifts:

$$\sigma_d = \frac{4\pi}{k^2}\sum_{l=0}^{\infty}(2l+1)\sin^2\delta_l , \tag{8}$$

$$\sigma_{\text{ex}} = \frac{4\pi}{k^2}\sum_{l=0}^{\infty}(-1)^l(2l+1)\sin^2\delta_l . \tag{9}$$

Here σ_d and σ_{ex} represent the direct and exchange cross sections, respectively. Recall that if the particles are distinguishable the total cross section is given by σ_d, while if the particles are indistinguishable the total cross section is $\sigma_d + \sigma_{\text{ex}}$.

For transport calculations of gases in thermal equilibrium at temperature T, a more useful quantity is the Boltzmann averaged cross section[16]

$$W^{(t,s)}[\sigma]=\int_0^\infty d\gamma e^{-\gamma^2}\gamma^{2s+3}Q^{(t)}(\gamma\tilde{k}) , \quad (10)$$

where we have defined $\tilde{k}=\sqrt{mkT}/\hbar$ and the angular average

$$Q^{(t)}(k)=2\pi\int_{-1}^{1} d(\cos\theta)(1-\cos^t\theta)\frac{d\sigma}{d\Omega}(k) . \quad (11)$$

For calculations of the thermal conductivity, $W^{(2,2)}$ will play the dominant role.

E. Simplifying assumptions

Throughout the remainder of this paper, we shall follow other authors in making several simplifying assumptions for transport calculations.

The experiments described in this paper were conducted on a nondegenerate Bose gas. The thermal de Broglie wavelength $\Lambda(T)=h/\sqrt{2\pi mkT}$ for the temperature range studied here was always several orders of magnitude smaller than the average interatomic spacing $r_0=n^{-1/3}$. Degeneracy effects related to the formation of the Bose condensate can therefore be ignored and we may use the Boltzmann transport equation to calculate the kinetic behavior of H↓.

We shall restrict our discussion to dilute gases ($a \ll r_0$). This ensures that we need to consider only binary collisions; multiatom scattering channels, though important for molecular recombination mechanisms, will be neglected in our calculations.

Note that for the low temperatures described in this paper, the s-wave channel is the dominant scattering process in the gas. In the low-energy and low-temperature limits, the relevant elastic cross sections become

$$\sigma_d,\sigma_{ex}\rightarrow 4\pi a^2, \quad k\rightarrow 0 , \quad (12)$$

$$W^{(2,2)}[\sigma_d], W^{(2,2)}[\sigma_{ex}]\rightarrow 8\pi a^2, \quad T\rightarrow 0 . \quad (13)$$

We shall report values of the thermal conductivity for the hydrodynamic regime ($\lambda \ll L$), where λ is the mean free path and L is the length scale of the macroscopic temperature gradient applied to the gas. For spin-polarized hydrogen, the mean free path may be estimated from the s-wave collision length:

$$\lambda=\frac{1}{\sqrt{2}}\frac{1}{n\sigma}\approx\frac{1}{8\sqrt{2}}\frac{1}{\pi na^2} . \quad (14)$$

In this expression, we approximate the total cross section by its $k=0$ value. Hence for a gas at $T=0.3$ K with number density $n=10^{16}$ atoms/cm^3, the mean free path is approximately 1 mm.

F. Paramagnetic Bose gas model

Lhuillier and Laloë modeled H↓ as a binary gas mixture of a and b atoms. Recall that, in the high-field limit, the proton spins serve to distinguish between the atoms, since the electron spins of the two states are both aligned antiparallel to the applied magnetic field.

Models that distinguish the a and b atoms predict transport phenomena that depend upon the nuclear polarization α, even though the dependence of the interatomic potential upon the proton spins has been neglected. This polarization-dependent behavior emerges solely from identical particle considerations. Collisions between pairs of a atoms or pairs of b atoms involve indistinguishable particles and have different elastic collision cross sections than those for a-b collisions, which are between distinguishable particles. Since α determines the ratio of a-a and b-b to a-b collisions, the effective overall cross section and hence the thermal conductivity depends upon the nuclear polarization of the gas.

Recall that the coefficient of thermal conductivity measures the ability of the gas to transport heat from hot to cold regions. The heat flux density $d\mathbf{q}/dt$ is defined to be the energy flow in the gas per unit time and unit area. For a slowly varying temperature distribution $T(\mathbf{r})$ in the gas, the heat flux density is directed opposite to the local temperature gradient

$$\frac{d\mathbf{q}}{dt}=-\kappa\nabla T , \quad (15)$$

where the proportionality constant is defined as the thermal conductivity κ. For a spinless monatomic gas, the thermal conductivity is given by[16]

$$\kappa_{\text{classical}}=\frac{25}{16}\frac{\sqrt{\pi mKT}}{W^{(2,2)}[\sigma]}\frac{c_v}{m}=\frac{25\pi}{32}n\bar{v}\lambda c_v . \quad (16)$$

Here the specific heat per atom is $c_v=3k/2$.

This simple classical approach must be extended for the treatment of quantum binary gases with spin. In a series of three papers in 1982, Lhuillier and Laloë developed a theory for transport in spin-polarized Boltzmann gases, one which included the identical particle effects outlined above. They explored the behavior of nondegenerate gases obeying either Fermi-Dirac or Bose-Einstein statistics. In their theory, the gas atoms all possess spin i and are distinguishable only by the quantum number m_i. Furthermore, Lhuillier and Laloë assumed that the interatomic potential was spin independent. We present here their calculations for spin-polarized hydrogen, a Bose gas indexed by the $i=\frac{1}{2}$ proton spins.

Solution of the Boltzmann equation for this model reveals that the thermal conductivity for the unpolarized gas ($\alpha=0$) is given by

$$\kappa_0=\frac{25}{16}\frac{\sqrt{\pi mkT}}{W^{(2,2)}[\sigma_d]+\frac{1}{2}W^{(2,2)}[\sigma_{ex}]}\frac{c_v}{m} . \quad (17)$$

The thermal conductivity in this model for a gas with arbitrary polarization is

$$\kappa(\alpha)=\kappa_0\frac{1-\xi_1\alpha^2}{1-\xi_2\alpha^2} . \quad (18)$$

The dimensionless quantities ξ_1 and ξ_2 are determined from the collisional cross sections $W^{(1,1)}[\sigma_d]$, $W^{(1,2)}[\sigma_d]$, $W^{(1,3)}[\sigma_d]$, $W^{(2,2)}[\sigma_d]$, and $W^{(2,2)}[\sigma_{ex}]$. In the $T\rightarrow 0$ limit, $\xi_1\rightarrow\frac{16}{75}$ and $\xi_2\rightarrow-\frac{11}{225}$.

The results for H↓ are displayed in Fig. 2. At temperature below 0.1 K, the temperature dependence of κ is due to the average velocity of the gas atoms. For higher tem-

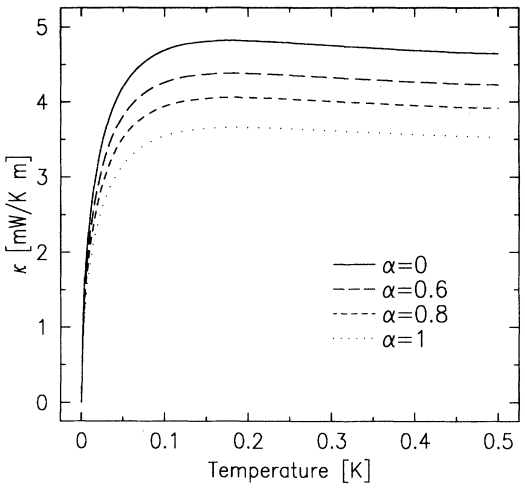

FIG. 2. Thermal conductivity as a function of temperature for the paramagnetic Bose gas model. Note that κ is suppressed for increasing nuclear polarization α.

peratures, κ deviates from $\sqrt{T}$ behavior and becomes nearly constant because of the compensating temperature dependence of the collisional cross sections. Note that as the nuclear polarization α increases, so do the number of collisions between identical particles, which in turn leads to larger effective cross sections in Bose gases like spin-polarized hydrogen. This reduces the length scale (the mean free path) over which heat is transported and hence suppresses the thermal conductivity κ. Since this model considered only the identical particle properties and not the magnetic characteristics of the atomic spins, Lhuillier and Laloë found transport behavior that is unaffected by the applied magnetic field.

An alternative theory including identical particle effects in spin-polarized Fermi gases was developed independently by Bashkin and Meyerovitch for dilute solutions of ^{3}He in superfluid ^{4}He.[17] Meyerovitch extended this calculation to the nondegenerate regime and found results for Fermi gases that agree exactly with the Fermi-Dirac calculations of Lhuillier and Laloë.[17]

G. Collective mode effects

While the paramagnetic Bose gas model of Lhuillier and Laloë investigated the binary elastic collision cross sections, a recent paper by Bashkin[4] considered the interaction of the atoms in a paramagnetic gas with the transverse thermal fluctuations of the magnetization. In particular, that paper discusses the effects that collective modes have upon the transport properties of a spin-polarized Boltzmann gas such as H↓. The model presented in that paper and summarized here considered collisions between hydrogen atoms and nuclear spin waves. Such collisions may also be thought of as the absorption or emission of a spin wave by a scattered atom.

The presence of nuclear (proton) spin waves in spin-polarized hydrogen is a well-understood phenomenon, both theoretically and experimentally. The presence of weakly damped oscillations of the transverse proton magnetization was predicted theoretically[18] for low-temperature samples of H↓ with high degrees of nuclear polarization. More specifically, nuclear spin waves were predicted to be weakly damped when

$$\frac{\alpha\Lambda(T)}{a} \gg 1 \ . \tag{19}$$

Furthermore, the dispersion relation for such collective oscillations was predicted to obey

$$\omega(k)=\frac{\gamma_p H_0}{\hbar}-D(\alpha)k^2 \ , \tag{20}$$

where γ_p is the proton gyromagnetic ratio, H_0 is the applied magnetic field, and $D(\alpha)$ is a complex-valued effective diffusion constant. These long-lived oscillations were observed as narrow beat frequencies in the free-induction decay signal of pulsed NMR experiments performed by workers at Cornell.[19]

Suppose that the spin-wave population is in thermal equilibrium at the temperature T of the gas. Furthermore, assume that we work in the high-field limit, where the spin-wave dispersion relation is dominated by the Larmor frequency term and is approximately independent of wave vector k. Under these conditions, Bashkin has computed the cross sections for absorption and emission of a spin wave to be

$$\sigma_{\rm abs}=16\pi a^2\alpha(N_0+1), \quad \sigma_{\rm em}=16\pi a^2\alpha N_0 \ , \tag{21}$$

where N_0 is the thermal occupation number for magnons

$$N_0=(e^{\gamma_p H_0/kT}-1)^{-1} \ . \tag{22}$$

In this model, the population of thermally excited spin waves determines the importance of the atom-spin-wave collision channel. These cross sections can be quite large for spin-polarized hydrogen, where nuclear polarizations can be created in excess of thermally induced polarizations. For a typical temperature $T=0.2$ K and nuclear polarization $\alpha=0.8$, these cross sections are nearly *2 orders of magnitude* larger than the s-wave scattering cross sections. These collisions should be the dominant mechanism for transport in highly nuclear polarized H↓.

Bashkin has shown that solution of the Boltzmann equation including only these atom-spin-wave cross sections leads to the following expression for the thermal conductivity:

$$\kappa=\frac{\sqrt{2}}{3\pi}\frac{\sqrt{\pi mkT}}{W^{(2,2)}[\sigma_d]+\frac{1}{2}W^{(2,2)}[\sigma_{\rm ex}]}\frac{c_v}{m} \times\left[\cosh\frac{\gamma_p H_0}{kT}-1+\frac{1}{\alpha}\sinh\frac{\gamma_p H_0}{kT}\right] . \tag{23}$$

For spin-polarized hydrogen, the Larmore energy is small compared to the thermal energy ($\gamma_p H_0 \ll kT$), so the thermal conductivity simplifies to

$$\kappa=0.19\kappa_0\frac{1}{\alpha}\frac{\gamma_p H_0}{kT} \ , \tag{24}$$

where κ_0 is the result for the unpolarized gas derived in the previous section.

The thermal conductivity for this model is plotted as a function of temperature for a gas in a 10-T magnetic field in Fig. 3(a). The approximate $T^{-1/2}$ temperature dependence differs from the paramagnetic Bose gas model since it also includes contributions from the population of the thermally excited spin waves. The variation of κ with α is markedly stronger than that calculated purely from binary gas effects.

The most striking characteristic of transport via atom-spin-wave collisions is the magnetic-field dependence of the thermal conductivity, which reflects the thermal population of magnons in the gas. This can be seen in Fig. 3(b), where the suppression of the transport coefficients is plotted as a function of the applied field H_0.

III. EXPERIMENTAL APPARATUS

The experimental apparatus used to make the measurements reported in this paper may be conveniently divided into four major components: the dilution refrigerator and superconducting magnet, the atomic hydrogen source, the thermal conductivity cell, and the pressure and temperature sensors. We shall discuss each of these systems in turn.

A. Dilution refrigerator and magnet

An overview of the experimental apparatus is shown in Fig. 4. Cryogenic temperatures are provided by a SHE model 430 dilution refrigerator with a circulation capacity of approximately 0.5 mmol/s. The magnetic field used for confinement of spin-polarized hydrogen is generated by an American Magnetics model 2268 NbTi superconducting solenoid with a 3-in.-diam bore. Operated in persistent current mode, it provides a maximum field of 8 T at 4.2 K and is homogeneous to 1 part in 10^5 in a 1-cm^3 volume about the solenoid center. The magnetic-field profile along the axis of the experiment is shown in Fig. 4.

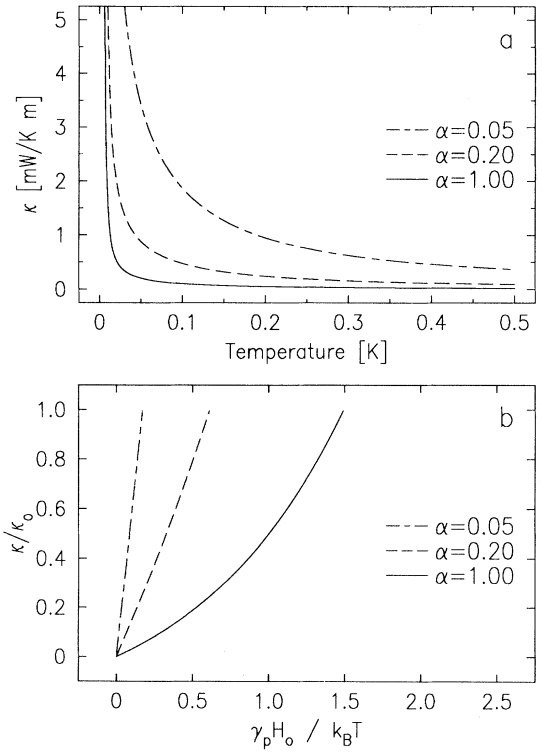

FIG. 3. (a) Thermal conductivity as a function of temperature for the a transport model that includes spin-wave effects. The magnetic field is taken to be 10 T. (b) Suppression of the thermal conductivity in this model as a function of the dimensionless parameter $\gamma_p H_0/kT$.

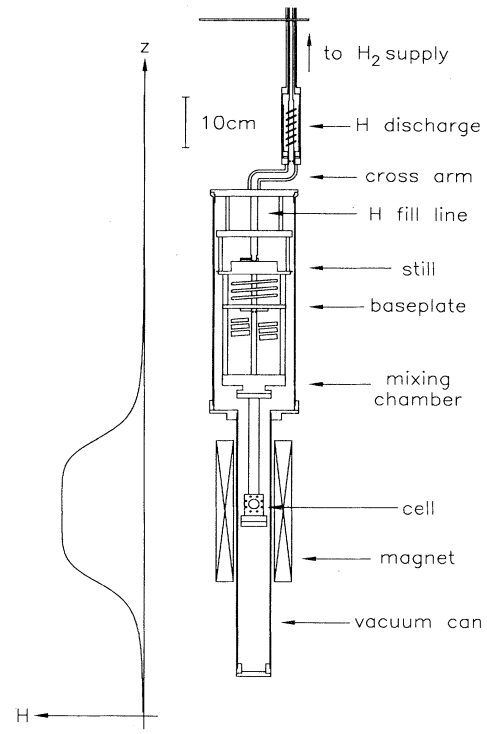

FIG. 4. Overview of the experimental apparatus. The magnetic field profile along the axis of the experiment is shown to the left of the drawing.

B. Atomic hydrogen source

Atomic hydrogen is produced from molecule hydrogen in a 77-K continuous wave radio frequency gas discharge. The connection between a room-temperature gas handling system and the discharge region is made through a 5-mm-i.d. Pyrex tube. At the discharge, this fill line expands to a 10-mm-i.d. Pyrex tube that lies along the axis of a helical $\lambda/4$ resonator coil. The resonator coil is composed of 30 tunes of 20-awg copper wire wound on a helical teflon coil form. Both fill tube and coil are immersed in a liquid-nitrogen reservoir.

A continuous flow of molecular H_2 gas at constant pressure (up to 3 torr) is sent down the Pyrex fill line. The application of approximately 10 W of resonant radio-frequency power generates electric fields inside the expanded fill tube which dissociate the molecular hydrogen into its atomic constituents. A portion of the atomic and molecular hydrogen exits the discharge region via the 1–2-mm-diam orifice at the base of the Pyrex tube.

The atomic hydrogen enters a 0.5-in.-diam stainless-steel cross arm immersed in the liquid-helium bath of the refrigerator. This cross arm is insulated from the liquid helium by a coating composed of Stycast 1266 epoxy[20] impregnated with 0.5-μm glass spheres. This cross arm connects the discharge region with an on-axis fill line that is thermally anchored to the stages of the dilution refrigerator en route to the experimental cell.

The operation of this atomic hydrogen source is described in detail elsewhere.[21] In the experiments described in this paper, the atomic hydrogen source delivered roughly $5-8\times10^{14}$ atoms per s to the experimental cell.

C. Thermal conductivity cell

The experimental cell is located at the mixing chamber terminus of the hydrogen fill line. It is mounted on an oxygen-free, high-conductivity (OFHC) copper support labeled in Fig. 5 as the multiport cell. The atomic hydrogen flux passes from the mixing chamber through a 0.438-in.-i.d. fill line to a rectangular copper block located at the center of the superconducting solenoid. This copper block has five circular measurement ports, one of each side and one on-axis port with bottom access. Three of the side ports are unused and are sealed with blank OFHC copper flanges.

The bottom port houses an OFHC copper assembly listed in Fig. 5 as the thermal conductivity insert. The insert possesses a coaxial cylinder geometry. The base of the insert forms an outer cylinder with radius $r_c=0.79$ cm and length 4.45 cm. This outer cylinder is thermally anchored to the multiport cell. The inner cylinder is a solid OFHC copper rod of radius $r_h=0.16$ cm and length $L=3.18$ cm. This rod is suspended by monofilament Kevlar thread[22] approximately 6 mm above the bottom of the outer cylinder. A chip resistor thermometer (see below) is located in each end of the inner cylinder. Although not shown, four coiled manganin wires, 0.0031 in. diameter and approximately 5 cm long when uncoiled, lead from each thermometer to an electrical feedthrough (also not shown) in the bottom of the outer cylinder, and ultimately to room-temperature electronics.

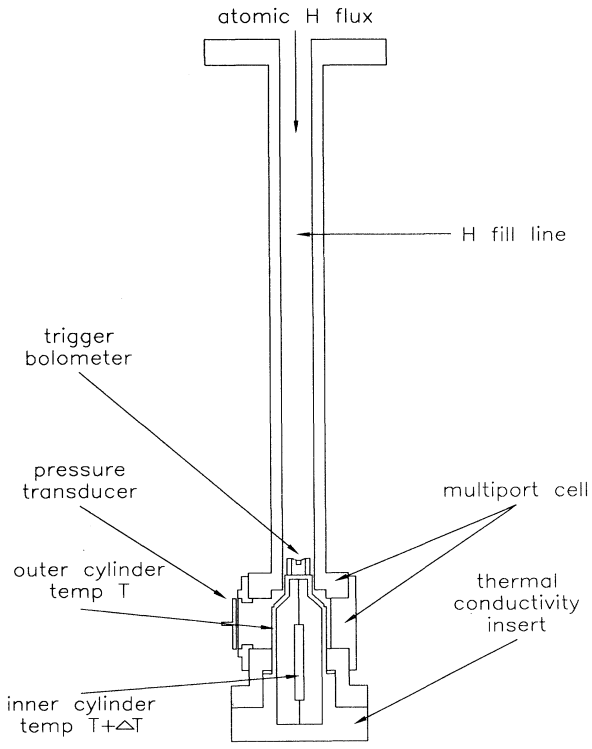

FIG. 5. Thermal conductivity cell.

This geometry ensures that the inner cylinder is thermally isolated from the outer cylinder and the rest of the experimental cell. Measurements with an empty cell indicate that the intrinsic heat leak from the central post to the base of the insert is on the order of 10^{-8} W/K. This occurs primarily through the coiled electrical leads.

This insert utilizes a modified hot wire technique to measure gaseous thermal conductivities. The outer cylinder is kept at constant temperature T by the dilution refrigerator, and the region between the two cylinders filled with spin-polarized hydrogen. The power $\dot{Q}$ necessary to maintain the inner cylinder at temperature $T+\Delta T$ is measured. When corrected for stray heat leaks, $\dot{Q}$ represents the heat transport by the gas from the hot inner cylinder to the cold outer cylinder. For small temperature differential ΔT in the hydrodynamic regime, the ratio $\dot{Q}/\Delta T$ is thus proportional to the thermal conductivity κ of the gas.

Each OFHC copper component of the cell was etched in a dilute solution of nitric acid to remove deposits from the machining process from the inner walls of the experimental cell. In addition, all surfaces in the experimental cell are coated with a saturated superfluid ^{4}He film during normal operation. A small puddle of liquid ^{4}He, typically less than 0.25 mm deep, forms in the base of the outer cylinder.

D. Pressure and temperature sensors

The pressure, and hence the density computed from the ideal gas law, of the spin-polarized hydrogen samples is measured by a capacitive pressure transducer mounted on the remaining side port of the experimental cell. This cryogenic pressure sensor is based upon a design first developed by Landau and coworkers.[23] The active element of the pressure transducer is a circular, 0.0005-in.-thick flexible Kapton[24] membrane. A 1.75-cm-diam electrode (50 Å chromium under 450 Å gold) is deposited on one side of the membrane. A 1.90-cm-diam circular brass fixed electrode is separated from the flexible electrode by an annular 0.5-ml Kapton spacer. The resulting parallel plate capacitor has a capacitance of approximately 60 pF at room temperature, with stray capacitances to ground of roughly 40 pF. Changes in the pressure of the gas in the cell produce deflections of the Kapton membrane, which in turn alters the capacitance of the pressure transducer.

The capacitance of the pressure transducer is measured by a cryogenic tunnel diode oscillator of the design developed by Van Degrift.[25] A biased tunnel diode (Gen-

eral Electric BD5) drives a resonant LC circuit composed of an isolation transformer and the pressure transducer. A small portion of the approximately 4.35-MHz resonance oscillation is leaked to two broadband 30 dB amplifiers (Avantek GPD201) in the room-temperature electronics. This amplified signal is mixed and filtered to a roughly 30-kHz oscillation whose frequency is measured by a Philips PM6654 frequency counter.

The response of the pressure transducer is calibrated for $0.2 \leq T \leq 0.4$ K against the saturated vapor pressure[26] of ^{3}He. The frequency deviation of the oscillator is linearly dependent upon the pressure to at least 50 mtorr, with a response of 114 ± 2 Hz per mtorr. The frequency of the pressure transducer-tunnel diode oscillator is stable to within 0.05 Hz, or 0.01 ppm of the resonance frequency, over several hours. The pressure transducer is hence sensitive to changes of 4×10^{-7} torr. For ideal gases at $T = 0.3$ K, this corresponds to density changes of 1×10^{13} cm^{-3}.

The baseline (empty cell) frequency of the pressure transducer varies slightly with the temperature of the mixing chamber. This is perhaps due to slight mechanical contraction in the isolation transformer or a small temperature dependence in the dielectric constant of the transformer coil form.

Primary thermometry is provided by a capacitive ^{3}He melting curve thermometer of the type developed by Greywall and Busch.[27] The thermometer is thermally anchored to the mixing chamber; its capacitance is measured by another tunnel diode oscillator. Pressures are measured to within 3 mbar, which corresponds to temperatures accurate to within 0.25 mK.

Secondary thermometry is provided by four wire resistance measurement of Dale Electronics model RCWP-575 1.00 kΩ 1% surface mount chip resistors. The temperature and magnetic field response of these thermometers has been reported by Li and coworkers.[28] Four chip thermometers are found throughout the experimental cell: one on the mixing chamber, one on the exterior of the thermal conductivity insert, and on each end on the inner cylinder of the thermal conductivity insert. In practice, one of the inner cylinder thermometers is used as a heater. The thermal contact between these thermometers and the central post itself is approximately 10^{-5} W/K and is primarily due to the bulk and surface thermal resistance of the intervening thin epoxy film used to affix the thermometers.

The mixing chamber and exterior insert thermometers are calibrated against the ^{3}He melting curve thermometer, while the central post thermometers are calibrated versus the mixing chamber thermometers with ^{3}He in the experimental cell. The high thermal conductivity of the helium vapor serves to lock the temperature of the inner cylinder to that of the outer cylinder.

IV. PROCEDURE

A. Theory of operation

In the measurements described in this paper, a sample of spin-polarized hydrogen is introduced to the experimental cell, where it fills the annular region between the inner and outer cylinders of the thermal conductivity insert. The mixing chamber, multiport cell, and outer cylinder are all maintained via a servo loop at a constant temperature T. A separate servo loop maintains the inner cylinder at a slightly warmer temperature $T+\Delta T$. The steady-state dc current $I_{\rm meas}$ and voltage $V_{\rm meas}$ supplies to the central post heater are measured in a standard four-wire configuration to eliminate the effects of lead resistances. The ohmic heating supplied to maintain the temperature differential ΔT is then

$$\dot{Q}_{\rm meas}(T,\Delta T,n)=I_{\rm meas}V_{\rm meas} \ . \tag{25}$$

As indicated above, $\dot{Q}_{\rm meas}$ varies with temperature, the temperature differential, and gas density. We then define $\dot{Q}_{\rm gas}$, the actual power conducted by the gas from inner to outer cylinder, by

$$\dot{Q}\text{gas}(T,\Delta T,n)=\dot{Q}_{\rm meas}-\Delta\dot{Q} \ , \tag{26}$$

where $\Delta\dot{Q}$ represents corrections due to stray heat leaks and external heat sources. We shall examine $\Delta\dot{Q}$ in more detail in Sec. V. For small temperature differentials, $\dot{Q}_{\rm gas}$ is proportional to ΔT so we define the thermal conductance (not to be confused with the thermal conductivity κ)

$$K_{\rm eff}(T,n)=\frac{\dot{Q}_{\rm gas}}{\Delta T} \ . \tag{27}$$

Note that $K_{\rm eff}$ is a function of the temperature and density of the gas.

The variation of $K_{\rm eff}$ with density may be divided into three transport regimes: ballistic (also known as free molecular), transition, and hydrodynamic. These regimes are characterized by the relative lengths of the mean free path λ and the transport distance d, which in our experimental cell is simply the distance (0.64 cm) between the inner and outer cylinders.

In the hydrodynamic regime ($\lambda \ll d$), heat conduction is completely governed by the many collisions required to traverse the transport distance. The thermal conductance is density independent and is proportional to the thermal conductivity κ. For a coaxial cylinder geometry ignoring end effects,

$$K_{\rm eff}^{\rm hyd}(n)=\frac{2\pi L\kappa}{\ln(r_c/r_h)} \ . \tag{28}$$

For rarified gases in the ballistic regime ($\lambda \gg d$), collisions play no role in heat transport. Instead, gas atoms carry energy directly from one wall to another. Further complicating the situation is the fact that gas atoms impinging upon a surface do not come into complete thermal equilibrium with the surface. One can phenomenologically describe the incomplete equilibration between gas a substrate by a single parameter a_c, known as the accommodation coefficient. For our experimental cell, heat transport is limited by the surface area of the inner cylinder and the thermal conductance in the ballistic regime may be written as

$$K_{\rm eff}^{\rm ball}(n)=a_c^{\rm eff}(2\pi r_h L)\left[\frac{n\bar{v}}{4}\right](2k) . \quad (29)$$

We have defined an effective accommodation coefficient $a_c^{\rm eff}$ which differs from a_c due to the following fact: the atoms carrying energy from one cylinder may fail to fully accommodate at the other cylinder and can actually return to redeposit their energy on the original surface. If the atoms scatter from the surfaces in a completely diffuse manner, then the effective accommodation coefficient reflects the relative surface areas of the inner and outer cylinders:

$$a_c^{\rm eff}=\frac{a_c}{1+(1-a_c)(r_h/r_c)} . \quad (30)$$

Note that $K_{\rm eff}$ is independent of the intrinsic thermal conductivity κ and is proportional to the density.

For intermediate densities in the transition regime ($\lambda\sim d$), the behavior of $K_{\rm eff}$ is more complicated. Both ballistic transport and collisions are important channels for heat conduction. Lees and Liu[29] and Lord[30] modeled this problem for a pair of concentric cylinders, and they found the best agreement with experimental data to be given by the form

$$K_{\rm eff}^{\rm trans}(n)=\left[\frac{1}{K_{\rm eff}^{\rm hyd}(n)}+\frac{1}{K_{\rm eff}^{\rm ball}(n)}\right]^{-1} . \quad (31)$$

The expression presented above were calculated for an ideal coaxial cylinder geometry and ignore end and off-axis alignment effects. Exact numerical solution of the temperature distribution including end effects in our experimental cell indicate that the thermal conductance in the hydrodynamic regime is 5% greater than the ideal result. In the ballistic regime, end effects merely introduce a correction from the area of the inner cylinder end caps, which also add a 5% upwards correction to the thermal conductance for our experimental cell.

Off-axis misalignment of the inner cylinder by a displacement x also slightly modifies our ideal results. In the hydrodynamics regime, transport without end effects becomes

$$K_{\rm eff}^{\rm hyd}=\frac{2\pi L\kappa}{\ln\delta} , \quad (32)$$

where the dimensionless parameter δ is given by

$$\delta=\frac{r_c^2+r_h^2-x^2+\sqrt{[r_c^2-(x+r_h)^2][r_c^2-(x-r_h)^2]}}{2r_c r_h} . \quad (33)$$

The ballistic regime result for an off-axis inner cylinder ignoring end effects is

$$K_{\rm eff}^{\rm ball}=a_c^{\rm eff}(2\pi r_h L)\zeta\left[\frac{n\bar{v}}{4}\right](2k) , \quad (34)$$

where the dimensionless parameter ζ is given by the integral

$$\zeta=\frac{1}{2\pi}\int_0^{2\pi}\left[\sin^2\phi+\left[\cos\phi-\frac{x}{r_c}\right]^2\right]^{-1/2}d\phi . \quad (35)$$

For our experimental cell, even an unreasonably large off-axis displacement of 0.2 cm (nearly a third of the separation between cylinders) introduces only a 4% increase in either regime from the ideal on-axis result.

B. Measurements

We performed a calibration check of our apparatus by measuring the thermal conductivity of gaseous ^{3}He for $0.3\le T\le 0.5$ K and gaseous ^{4}He for $0.75\le T\le 0.9$ K. Our measurements, reported elsewhere,[31] were in excellent agreement with both *ab initio* theoretical calculations[32,33] and previous experimental results[34] at higher temperatures. These measurements suggest that systematic errors associated with our experimental apparatus are less than 5%.

We then performed heat transport measurements of spin-polarized hydrogen in a 7.00-T magnetic field for temperatures ranging from 0.2 to 0.4 K, and at 0.37 K for magnetic fields from 3.00 to 7.00 T. We measured thermal transport for samples with densities up to 2×10^{16} cm^{-3} and nuclear polarizations up to 98%.

At each value of the temperature and magnetic field, we performed measurements according to the following procedure. We generate the standard temperature differential in the experimental cell (outer cylinder temperature T, inner cylinder temperature $T+\Delta T$). Before introducing any H$\downarrow$ into the experimental cell, we measure baseline values of the central post heater current $I_{\rm base}$ and voltage $V_{\rm base}$. We then operate the hydrogen discharge and fill the cell with $H\downarrow$. When the density has reached a suitable initial level, we turn off the discharge. Due to well-understood recombination and relaxation processes in the gas, the sample will decay with lifetimes ranging from one to several hours. We periodically record the pressure p of the gas, the temperatures $T_{\rm inner}$ and $T_{\rm outer}$ of the coaxial cylinders, and the current $I_{\rm meas}$ and voltage $V_{\rm meas}$ applied to the inner cylinder heater. These measurements were generally repeated every 10 seconds. Measurement data are shown in Fig. 6 for a H$\downarrow$ sample created at $T=0.309$ K and $H=7.00$ T.

Since collision times in H$\downarrow$ are rapid (10μs) in comparison to the density decay times (10^2–10^4 s), we expect that these H$\downarrow$ samples are always in thermal equilibrium. Our measurements of $\dot{Q}_{\rm meas}(t)$ then represent the steady-state transport for a gas at density $n(t)$.

For all of the H$\downarrow$ measurements, the experimental cell and lower fill line are coated with a saturated superfluid ^{4}He film. We create this film by introducing 99.99% purity ^{4}He gas from a room-temperature gas handling system. The gas is cryopumped into the hydrogen fill line and the experimental cell; at dilution refrigerator temperatures, it condenses upon the inner surfaces of the fill line and cell. Approximately 16 mmol of ^{4}He gas is required to form a saturated film for our experimental apparatus. We attribute this relatively large quantity of helium to the extensive surface area of the copper sinter in the fill line. We qualitatively monitor the film thickness in the

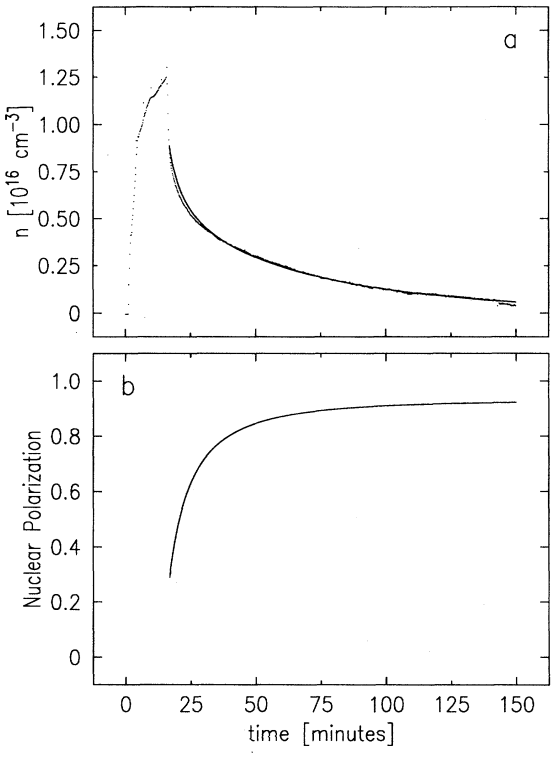

FIG. 6. Pressure, temperature, and applied power data taken for a H↓ sample at $T=0.309$ K and $H=7.00$T.

experimental cell by measuring the energy required to heat and completely evaporate the helium film from the inner cylinder.

V. RESULTS

In this section we describe the procedure used to extract the thermal conductivity $\kappa(T)$ and accommodation coefficient $a_c(T)$ from the experimental data.

A. Density $n(t)$ and nuclear polarization $\alpha(t)$

We determine the development of the nuclear polarization $\alpha(t)$ of a H↓ sample directly from the time evolution of the density $n(t)$. This is possible because the rate constants of the relaxation and recombination processes are well known.

We model the H↓ sample as a binary gas of a and b atoms with densities n_a and n_b. The time evolution of this gas is then governed by the coupled first-order differential equations:

$$-\frac{dn_a}{dt}=R(n_a-n_b)+2K_{aa}n_a^2+K_{ab}n_an_b +(G_s+G_b)(n_a^2-n_b^2)\ ,$$
$$-\frac{dn_b}{dt}=R(n_b-n_a)+K_{ab}n_an_b+(G_s+G_b)(n_b^2-n_a^2)\ . \tag{36}$$

R is the one-body relaxation rate constant, K_{aa} and K_{ab} are the two-body recombination rate constants, and G_b and G_s are the two-body relaxation rate constants in the bulk and on the surface. K_{aa}, K_{ab}, G_b, and G_s are completely determined[35,21] from the temperature, the magnetic field, and the area to volume ratio of the experimental cell ($A_{\rm cell}/V_{\rm cell}=5.94$ cm^{-1}). The surface two-body relaxation rate constant G_s also depends upon the angle between the magnetic field and the surface normal. Since the surfaces inside the experimental cell do not possess any predominant orientation with respect to the magnetic field, we have chosen to use the angular average of G_s. In this model we have also ignored three-body recombination processes, as they become important only for densities greater than 10^{17} cm^{-3}.

We determine the nuclear polarization $\alpha(t)$ by matching the observed density decay $n(t)=p/kT$ with the simulated total density $n_{\rm sim}(t)=n_a+n_b$ determined from this model. Only two parameters are adjusted: the initial nuclear polarization and the one-body relaxation rate R. The initial total density is determined from the observed decay profile. The nuclear polarization is then easily found from the a and b densities:

$$\alpha(t)=\frac{n_b-n_a}{n_b+n_a}\ . \tag{37}$$

The density $n(t)$ and the nuclear polarization $\alpha(t)$ calculated in this fashion for a $T=0.309$ K and $H=7.00$ T gas is shown in Fig. 7. Slight discrepancies between experimental data and our model (such as those observable

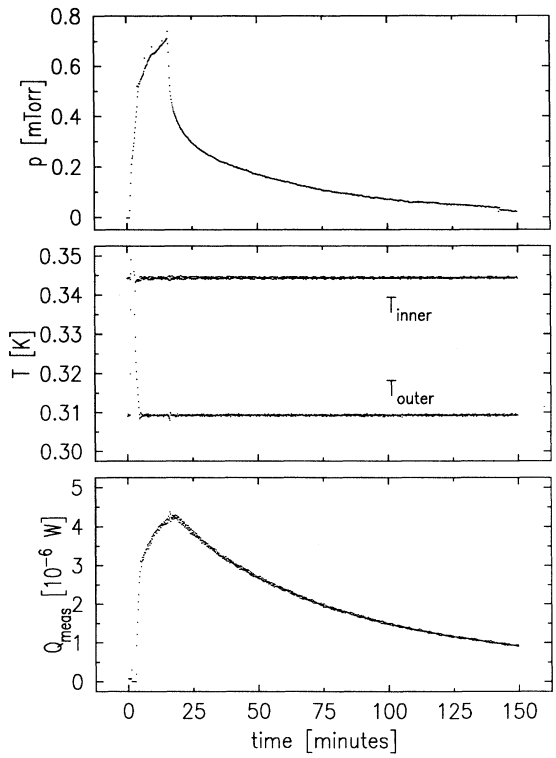

FIG. 7. The time evolution of the density (a) and nuclear polarization (b) of a H↓ sample. Plotted points represent measurements, solid lines represent the results of the model described in the text.

in the figure near $t=25$ min) represent uncertainties of approximately 5% in our determination of the nuclear polarization α.

B. Power corrections $\Delta\dot{Q}$

For our measurements of the thermal transport in spin-polarized hydrogen, it is important to note that the H↓ gas transports heat from the inner cylinder's helium film to the outer cylinder's helium film. Corrections $\Delta\dot{Q}$ to the measured power $\dot{Q}_{\rm meas}$ must not only include the effects of the intrinsic cell heat leak and electrical noise, but also include heat flow through the helium film as well as heat deposited by the formation of molecular H_2 during the decay of a H↓ sample. These corrections are illustrated in the block diagram in Fig. 8.

In this block diagram, $\dot{Q}_{\rm leak}$ and $\dot{Q}_{\rm noise}$ represent the intrinsic cell heat leak and electrical noise corrections, $\dot{Q}_{\rm film}$ represents the heat leak through the ^{4}He film, and $\dot{Q}_{\rm rec}^{\rm inner}$ and $\dot{Q}_{\rm rec}^{\rm outer}$ represent the recombination heat deposited on both the inner and outer cylinder helium films. One can see from the diagram that the actual heat flux transported by the gas is given by $\dot{Q}_{\rm gas}=\dot{Q}_{\rm meas}-\Delta\dot{Q}$, where

$$\Delta\dot{Q}=\dot{Q}_{\rm leak}-\dot{Q}_{\rm noise}+\dot{Q}_{\rm film}-\dot{Q}_{\rm rec}^{\rm inner} . \tag{38}$$

We have determined the first three terms in the above expression experimentally. The baseline heat leak $I_{\rm base}V_{\rm base}$, measured prior to the introduction of H↓, includes $\dot{Q}_{\rm film}$ as well as the other hydrogen-independent terms $\dot{Q}_{\rm leak}$ and $\dot{Q}_{\rm noise}$. Recent measurement of the H-He cross section[36] suggest that $\dot{Q}_{\rm film}$ is only very weakly dependent upon the hydrogen density for our experimental conditions. We may replace all three by this measured baseline heat leak:

$$\dot{Q}_{\rm leak}-\dot{Q}_{\rm noise}+\dot{Q}_{\rm film}=I_{\rm base}V_{\rm base} . \tag{39}$$

These baseline powers are roughly 100 nW at 0.4 K, but drop to 5 nW at 0.2 K.

The remaining term in $\Delta\dot{Q}$ arises from the decay of the spin-polarized hydrogen sample. Each hydrogen atom that is lost to the H↓ gas becomes one half of a H_2 molecule, which promptly freezes on the surfaces of the experimental cell. During this process, 4.8 eV of recombination energy is released per molecule. As the H↓ sample decays, the total recombination power produced in the cell by the formation of molecular hydrogen is given by

$$\dot{Q}_{\rm rec}^{\rm tot}=\frac{4.8\ {\rm eV}}{2}V_{\rm cell}\frac{dn}{dt} , \tag{40}$$

where $V_{\rm cell}=25.0$ cm^3 is the volume of the experimental cell. If we assume that the recombination power is deposited uniformly across the surfaces of the experimental cell, the power deposited upon the inner and outer cylinders is given by

$$\dot{Q}_{\rm rec}^{\rm inner}=\frac{A_{\rm inner}}{A_{\rm inner}+A_{\rm outer}}\dot{Q}_{\rm rec}^{\rm tot}$$

and

$$\dot{Q}_{\rm rec}^{\rm outer}=\frac{A_{\rm outer}}{A_{\rm inner}+A_{\rm outer}}\dot{Q}_{\rm rec}^{\rm tot} , \tag{41}$$

where $A_{\rm inner}=3.33$ cm^2 and $A_{\rm outer}=145.3$ cm^2 are the surface areas of the inner cylinder and the outer cylinder assembly (outer cylinder, multiport cell, and fill line). As much as 100 μW is deposited on the cell surfaces during the initial rapid recombination segment of $n(t)$; 100 nW is typical for the relaxation bottlenecked regime where values of dn/dt are considerably smaller.

C. Temperature differential ΔT

The true temperature differential across the gas is not the temperature difference of the inner and outer cylinders, but the difference in the helium film temperatures:

$$\Delta T=T_{\rm inner}^{\rm film}-T_{\rm outer}^{\rm film} . \tag{42}$$

We have been careful to distinguish the film temperature from the temperature of the underlying substrate because of the presence of a thermal boundary resistance, known as the Kapitza resistance. The Kapitza resistance is inversely proportional to the area of the boundary and is due to the mismatch of phonon dispersion relations in the helium film and the OFHC copper substrate. For bulk liquid ^{4}He and copper, the Kapitza thermal resistivity is given in the 0.2–0.5 K temperature range by the expression[37]

$$R_K(T)=\frac{4.0\times10^{-3}\ {\rm m^2K^4/W}}{T^3} . \tag{43}$$

Since the power transported across the inner cylinder-helium film boundary is $\dot{Q}_{\rm meas}-\dot{Q}_{\rm leak}+\dot{Q}_{\rm noise}$, the temperature differential at the inner cylinder is

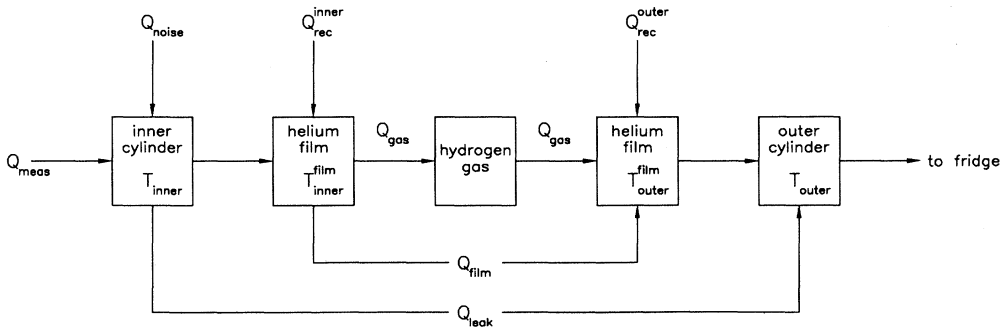

FIG. 8. Block diagram of power and temperature corrections.

$$T_{\text{inner}} - T_{\text{inner}}^{\text{film}} = R_K A_{\text{inner}} (\dot{Q}_{\text{meas}} - \dot{Q}_{\text{leak}} + \dot{Q}_{\text{noise}}) . \quad (44)$$

Similarly, the temperature differential at the outer cell is

$$T_{\text{outer}}^{\text{film}} - T_{\text{outer}} = R_K A_{\text{outer}} (\dot{Q}_{\text{meas}} - \dot{Q}_{\text{leak}} + \dot{Q}_{\text{noise}} + \dot{Q}_{\text{rec}}^{\text{tot}}) . \quad (45)$$

These temperature corrections are important only in the rapid recombination segment of a H↓ sample decay; even then these corrections are less than 2 mK. In general, our measurements were taken for temperature differentials ΔT between 20 and 40 mK.

D. Thermal conductance $K_{\text{eff}}(n)$

Once the power $\dot{Q}_{\text{gas}}$ and temperature differential ΔT across the spin-polarized hydrogen sample are determined, the thermal conductance $K_{\text{eff}} = \dot{Q}_{\text{gas}} / \Delta T$ is easily computed. Recall however that our expressions for $K_{\text{eff}}(n)$ in terms of the thermal conductivity κ and the effective accommodation coefficient a_c are valid only when $\dot{Q}_{\text{gas}}$ is proportional to the temperature differential ΔT. We verified that our measurements are indeed within this linear regime. For temperature differentials up to approximately 40 mK, we found K_{eff} to be independent of the temperature differential.

E. Accommodation coefficient a_c

The effective accommodation coefficient a_c^{eff} may be calculated from the behavior of $K_{\text{eff}}(n)$, particularly at low density. Recall that the density variation of the thermal conductance may be written

$$\frac{1}{K_{\text{eff}}(n)} = A + \frac{B}{n} , \quad (46)$$

where the definitions of the parameters A and B in terms of the thermal conductivity κ and effective accommodation coefficient a_c^{eff} are

$$A = \frac{\ln(r_c / r_h)}{2\pi L \kappa}$$

and (47)

$$B = \frac{1}{a_c^{\text{eff}} (2\pi r_h L)(\bar{v}/4)(2k)} .$$

In order to determine a_c^{eff}, we determine the best least-squares linear fit to $1/K_{\text{eff}}$ versus $1/n$, and extract the effective accommodation coefficient from the slope B.

The intrinsic accommodation coefficient a_c is then given by

$$a_c = a_c^{\text{eff}} \frac{1 + r_h / r_c}{1 + a_c^{\text{eff}} r_h / r_c} . \quad (48)$$

Computations of a_c for each H↓ sample are collected and displayed in Fig. 9.

Our results for the accommodation coefficient of H↓ on saturated superfluid ^{4}He films for $0.2 < T < 0.4$ K are in good agreement with previous measurements. In this regime, we find that $a_c(T) = (0.56 \pm 0.06) T$ where the temperature T is expressed in K. The uncertainty in $a_c(T)$ arises from the scatter in the data. Helffrich and coworkers[5] have measured the accommodation coefficient on helium surfaces for 0.1–0.4 K using a parallel plate geometry and found $a_c(T) = 0.50T$.

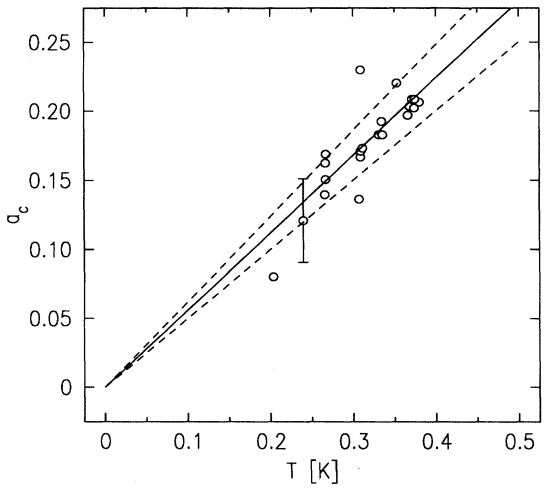

FIG. 9. Accommodation coefficient of H↓ on superfluid ^{4}He films as a function of temperature. The solid line $a_c(T) = 0.56T$ represents the least-squares linear fit. The dashed lines $a_c(T) = 0.50T$ and $a_c(T) = 0.62T$ indicate uncertainty in the linear dependence of the accommodation coefficient.

These results for the accommodation coefficient are also in close agreement with values of the sticking probability $s(T)$ for this temperature regime. Theoretical calculations[38,39] and experimental measurements[6] of the sticking probability for $0.15 < T < 0.53$ K report $s(T) = 0.33T - 0.35T$. These measurements correspond to accommodation coefficients $a_c(T) = 0.50T - 0.53T$, which are in excellent agreement with the measurements by Helffrich *et al.* and the measurements reported in this paper. Although recent work by Berkhout and Walraven[40] suggest that the sticking probability is given by $s = 0.65T$ in this temperature regime, this is not in agreement with accommodation coefficient measurements.

Note that the accommodation coefficient is found to be independent of the applied magnetic field (see Fig. 10). This is not surprising, as the van der Waals interaction between the incident hydrogen atom and the superfluid ^{4}He surface is independent of the proton and electron spins of the hydrogen atom.

F. Thermal conductivity κ

The thermal conductivity κ may be extracted from the behavior of $K_{\text{eff}}(n)$ in the transition and hydrodynamic regimes. Recall that

$$\frac{n}{K_{\text{eff}}} = An + B , \quad (49)$$

where A and B are defined as before. If we fit the behavior of n/K_{eff} versus n to a straight line with fixed intercept B (as determined during calculations of a_c^{eff}),

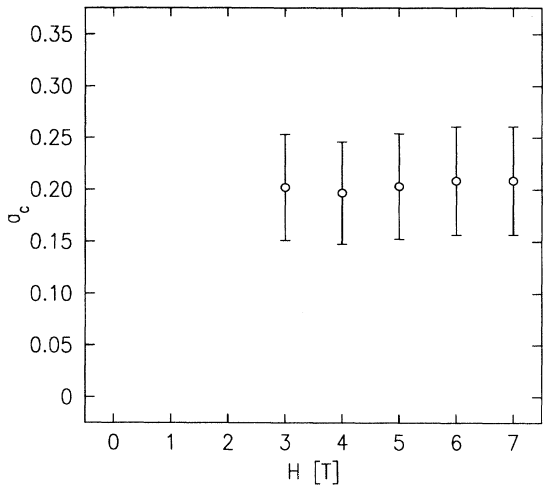

FIG. 10. Magnetic field dependence at 0.37 K of a_c for H↓ on superfluid ^{4}He films.

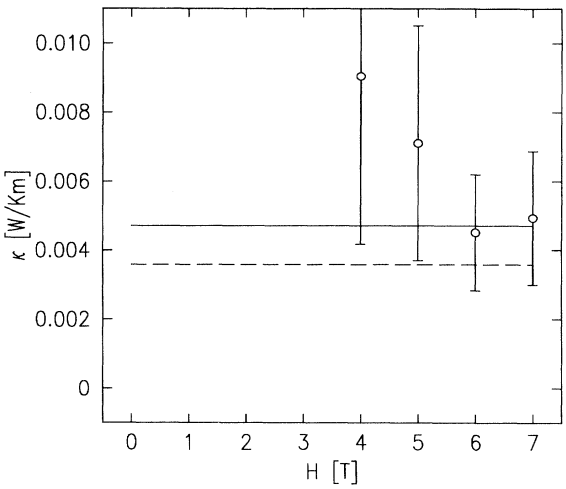

FIG. 12. Thermal conductivity of H↓ as a function of magnetic field for $T=0.370$ K. The solid and dashed lines represent the thermal conductivities for the unpolarized and completely polarized binary gas model.

the slope A is inversely proportional to the thermal conductivity κ. We perform these calculations for every H↓ sample that enters the transition regime (densities $n > 8\times10^{15}$ cm^{-3}); the results for $\kappa(T)$ are shown in Figs. 11 and 12.

Our results for the thermal conductivity represent the first measurements of thermal transport in gaseous spin-polarized hydrogen. As one can see in Fig. 11, the behavior of κ for H↓ samples at 7.00 T are in rough agreement with the calculations by Lhuillier for an unpolarized binary Bose gas indexed by the nuclear spin $i=\frac{1}{2}$, which suggests that distinguishability effects for the a and b atoms in H↓ may indeed be important for thermal transport at these temperatures.

The lack of samples of H↓ with both high-density and high nuclear polarization does not allow us to comment upon the polarization dependence of κ. The data reduction technique outlined in the previous section assumed that the thermal conductivity κ remained constant during a sample decay. Since the nuclear polarization α in fact evolves from 0% to nearly 100% during a sample decay, our technique is not strictly accurate if we consider the possibility that κ is a function of α. However, if we model the polarization dependence of the thermal conductivity by the weakly varying Lhuillier and Laloë result for the binary gas model

$$\kappa(\alpha)=\kappa_0\frac{1-\xi_1\alpha^2}{1-\xi_2\alpha^2}\ , \tag{50}$$

we cannot distinguish the predicted behavior of K_{eff} from our polarization-independent calculations (see Fig. 13) within the measurement error.

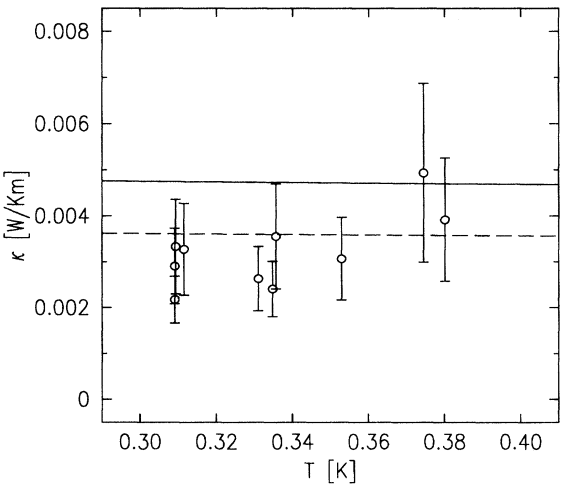

FIG. 11. Thermal conductivity of H↓ as a function of temperature for $H=7.0$T. The solid and dashed lines represent the thermal conductivities for the unpolarized and completely polarized binary gas model.

The apparent magnetic field dependence of the thermal conductivity is inconclusive, due to the large error bars on the data at low magnetic field. The large uncertainties are due to the fact that these samples were at lower density and do not extend very far into the transition regime where thermal conductivities κ are easily determined. Recall that in the binary gas model the thermal conductivity is independent of the magnetic field. In the binary gas model, the electron and proton spins affect the thermal transport only through quantum indistinguishability effects, and the predicted transport coefficients are independent of the magnetic field. If the thermal conductivity is truly dependent upon the magnetic field, perhaps spin-dependent contributions to the H-H interaction potential must be considered in models of transport in spin polarized hydrogen.

However, we can conclude that anomalies in the thermal transport due to spin-wave effects are not observed in spin-polarized hydrogen. None of the expected signatures of spin-wave-moderated transport—suppression of κ by 2 orders of magnitude, linear depen-

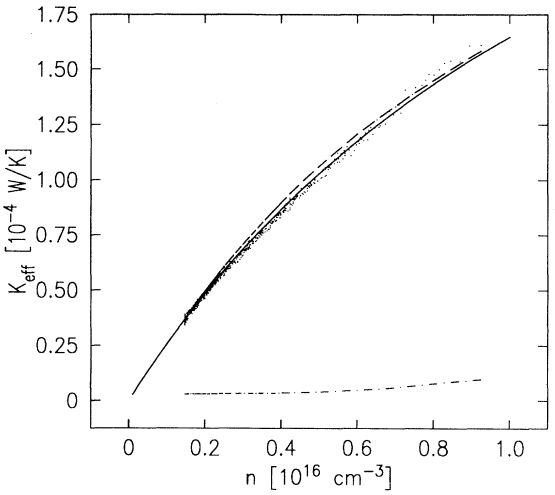

FIG. 13. $K_{\text{eff}}(n)$ for H↓ at 0.309 K and 7.00T. The solid line indicates the behavior of K_{eff} for polarization-independent thermal conductivity α. The dashed line is the behavior of K_{eff} for the binary gas model. The dash-dotted line represents the predicted behavior of K_{eff} for the spin-wave-moderated transport model.

dence upon the magnetic field, and strong dependence on the nuclear polarization—were observed. To illustrate this fact, the expected behavior of $K_{\text{eff}}(n,\alpha)$ for this transport model is shown by the dash-dotted line in Fig. 13. In addition, the thermal conductivity κ appears to decrease with increased magnetic field; exactly the opposite effect to that predicted by the spin-wave transport model.

Recall, however, that the theoretical calculations of spin-wave-moderated transport assumed a magnon population in thermal equilibrium with the gas. If thermal equilibration times for spin waves in H↓ are long compared with density decay times (10^4 s), then it is possible that thermal magnon populations never naturally evolve in H↓. In any event, it is clear that a reevaluation of this transport model is warranted by the experimental results presented here.

VI. CONCLUSION

The measurements described in this paper have clearly shown that thermal transport in H↓ is governed by diffusive collisions and strongly suggest that identical particle effects play a role in determining the elastic collision cross sections in the gas. Furthermore, our results demonstrate that dramatically enhanced scattering due to collective effects does not occur in H↓.

A close reexamination of the collective effects transport model proposed by Baskin is certainly warranted by our experimental results. Definitive conclusions regarding other models of thermal transport in H↓ must wait for precise measurements of the variation of κ with nuclear polarization and applied magnetic field. Such measurements require the production of highly nuclear polarized samples with densities deep into the transition regime, and preferably in the hydrodynamic regime. The most direct route to the production of such samples involves the combination of a larger measurement cell and a more prolific atomic hydrogen source, which in turn requires a dilution refrigerator with greater cooling power.

Measurements of other transport coefficients in the gas, such as the viscosity η, should also provide insights into the elastic collision mechanisms in spin-polarized hydrogen. In principle, experiments involving the damping by the gas of a vibrating wire or cylinder would allow one to measure the viscosity of the gas. However, geometric constraints may make such experiments infeasible.

ACKNOWLEDGMENTS

This work was supported by the National Science Foundation through Grant No. DMR-91-19426. One of us (M.J.Y.) acknowledges the support of the National Science Foundation. We would like to thank D. Kleppner, J. M. Doyle, J. C. Sandberg, I. A. Yu, and C. L. Cesar for helpful discussions.

*Present address: AT&T Bell Laboratories, Murray Hill, New Jersey 07974.

[1]R. D. Etters, J. V. Dugan, Jr., and R. W. Palmer, J. Chem. Phys. **62**, 313 (1974).
[2]W. C. Stwalley and L. H. Nosanow, Phys. Rev. Lett. **36**, 910 (1976).
[3]C. Lhuillier, J. Phys. (Paris) **44**, 1 (1983).
[4]E. P. Bashkin, Phys. Rev. B **44**, 12 440 (1991).
[5]J. A. Helffrich, M. P. Maley, and M. Krusius, Phys. Rev. B **42**, 2003 (1990).
[6]J. J. Berkhout, E. J. Wolters, R. van Roijen, and J. T. M. Walraven, Phys. Rev. Lett. **57**, 2387 (1986).
[7]I. F. Silvera and J. T. M. Walraven, Phys. Rev. Lett. **44**, 164 (1980).
[8]T. J. Greytak and D. Kleppner, in *New Trends in Atomic Physics,* edited by G. Grynberg and R. Stora (North-Holland, Amsterdam, 1982).
[9]I. F. Silvera and J. T. M. Walraven, in *Progress in Low Temperature Physics,* edited by D. F. Brewer (Elsevier, Amsterdam, 1986), Vol. X.
[10]W. Kolos and L. Wolniewicz, J. Chem. Phys. **43**, 2429 (1965).
[11]W. Kolos and L. Wolniewicz, J. Chem. Phys. **49**, 404 (1968).
[12]W. Kolos and L. Wolniewicz, Chem. Phys. Lett. **24**, 457 (1974).
[13]W. Kolos and L. Wolniewicz, J. Mol. Spectrosc. **54**, 303 (1975).
[14]D. G. Friend and R. D. Etters, J. Low Temp. Phys. **39**, 409 (1980).
[15]L. J. Lantto and R. M. Nieminen, J. Low Temp. Phys. **37**, 1 (1979).
[16]J. O. Hirschfelder, C. F. Curtiss, and R. B. Bird, *Molecular Theory of Gases and Liquids* (Wiley, New York, 1954).
[17]E. P. Bashkin and A. E. Meyerovich, Adv. Phys. **30**, 1 (1981).
[18]E. P. Bashkin, Pis'ma Zh. Eksp. Teor. Fiz. **33**, 11 (1981) [JETP Lett. **33**, 8 (1981)].
[19]B. R. Johnson *et al.*, Phys. Rev. Lett. **52**, 1508 (1984); **53**, 302

(1984).
[20]Product of Emerson and Cuming, Inc., Canton, Massachusetts.
[21]D. A. Bell *et al.*, Phys. Rev. B **34**, 7670 (1986).
[22]Product of E. I. duPont de Nemours and Co., Wilmington, Delaware.
[23]J. Landau, J. T. Tough, N. R. Brubaker, and D. O. Edwards, Rev. Sci. Instrum. **41**, 444 (1970).
[24]Product of E. I. duPont de Nemours and Co., Wilmington, Delaware.
[25]C. T. Van Degrift, Rev. Sci. Instrum. **46**, 599 (1975).
[26]S. G. Sydoriak and R. H. Sherman, J. Res. Nat. Bur. Std. **68A**, 579 (1962).
[27]D. S. Greywall and P. A. Busch, J. Low Temp. Phys. **46**, 451 (1982).
[28]Q. Li *et al.*, Cryogenics **26**, 467 (1986).
[29]L. Lees and C.-Y. Liu, Phys. Fluids **5**, 1137 (1962).
[30]R. Lord, Phys. Fluids **11**, 1830 (1968).
[31]M. J. Yoo and T. J. Greytak (unpublished).
[32]W. E. Keller, Phys. Rev. **105**, 41 (1957).
[33]L. Monchick, E. A. Mason, R. J. Munn, and F. J. Smith, Phys. Rev. **139**, A1076 (1965).
[34]K. Fokkens, W. Vermeer, K. W. Taconis, and R. de Bruyn Ouboter, Physica **30**, 2153 (1964).
[35]J. P. H. W. van den Eijnde, Ph.D. thesis, Eindhoven University of Technology, The Netherlands, 1984.
[36]J. Mester, Ph.D. dissertation, Harvard University, 1992.
[37]F. Pobell, *Matter and Methods at Low Temperatures* (Springer-Verlag, New York, 1992).
[38]D. S. Zimmerman and A. J. Berlinsky, Can. J. Phys. **61**, 508 (1983).
[39]B. W. Statt, Phys. Rev. B **32**, 7160 (1985).
[40]J. J. Berkhout and J. T. M. Walraven, Phys. Rev. B **47**, 8886 (1993).